

Thermal Response and TCf of GaN/AlN Heterostructure Multimode Micro String Resonators From $-10\text{ }^{\circ}\text{C}$ Up to $325\text{ }^{\circ}\text{C}$

Wen Sui¹, Graduate Student Member, IEEE, Xu-Qian Zheng¹, Member, IEEE, Ji-Tzuoh Lin², Bruce W. Alphenaar², Member, IEEE, and Philip X.-L. Feng², Senior Member, IEEE

Abstract—We report on the first experimental characterization and analysis of the thermal response and temperature coefficient of resonance frequency (TCf) of gallium nitride/aluminum nitride (GaN/AlN) heterostructure micro string resonators, in a wide temperature range from $-10\text{ }^{\circ}\text{C}$ up to $325\text{ }^{\circ}\text{C}$. Thanks to its excellent electrical and mechanical properties and chemical inertness, GaN has recently stimulated growing interests in GaN microelectromechanical systems (MEMS) for emerging high-power, high-temperature, and harsh-environment applications. GaN films on Si wafers often require AlN buffer layers, thus the residual tensile stress profile in the GaN epilayers and GaN/AlN hetero-layers can play a key role in affecting the MEMS specifications and performance. Here we design and fabricate GaN/AlN heterostructure micro string resonators with length $L = 100, 200$ and $300\text{ }\mu\text{m}$ to probe the stress and thermal effects on resonance behavior. All out-of-plane flexural modes show clear string behavior, and the multimode resonance frequencies downshift almost linearly with increasing temperature up to $325\text{ }^{\circ}\text{C}$. The linear temperature dependence and TCf values of GaN/AlN heterostructure resonators can be directly employed for thermal sensing. Comparison among different devices indicates that higher tensile stress levels contribute to smaller TCf values, suggesting strain engineering may be exploited for intentionally regulating the TCf . [2021-0068]

Index Terms—GaN, GaN/AlN heterostructure, resonator, temperature coefficient of resonance frequency (TCf), multimode, string, stress, thermal expansion.

I. INTRODUCTION

GROUP III-nitrides, such as gallium nitride (GaN) and aluminum nitride (AlN), have attracted considerable attention as promising materials for high-power and ultrahigh-frequency electronics due to their appealing electrical properties, including intrinsic direct bandgaps, excellent breakdown

Manuscript received March 30, 2021; revised May 27, 2021; accepted June 5, 2021. Date of publication June 25, 2021; date of current version July 30, 2021. This work was supported by the Defense Threat Reduction Agency (DTRA) Basic Scientific Research Program under Grant HDTRA1-19-1-0035 and Grant HDTRA1-15-1-0027. Subject Editor D. Senesky. (Corresponding author: Philip X.-L. Feng.)

Wen Sui, Xu-Qian Zheng, and Philip X.-L. Feng are with the Department of Electrical and Computer Engineering, Herbert Wertheim College of Engineering, University of Florida, Gainesville, FL 32611 USA (e-mail: wen.sui@ufl.edu; xuqian.zheng@ufl.edu; philip.feng@ufl.edu).

Ji-Tzuoh Lin and Bruce W. Alphenaar are with the Department of Electrical and Computer Engineering, University of Louisville, Louisville, KY 40292 USA (e-mail: jitzuoh.lin@louisville.edu; bruce.alphenaar@louisville.edu).

Color versions of one or more figures in this article are available at <https://doi.org/10.1109/JMEMS.2021.3089703>.

Digital Object Identifier 10.1109/JMEMS.2021.3089703

1057-7157 © 2021 IEEE. Personal use is permitted, but republication/redistribution requires IEEE permission. See <https://www.ieee.org/publications/rights/index.html> for more information.

TABLE I
KEY MATERIAL PROPERTIES OF AlN AND GaN

Material	Young's Modulus [GPa]	Band Gap [eV]	Piezo-electric Constant [pm/V]	Thermal Conductivity [W/(m·K)]	Acoustic Velocity [m/s]
AlN	283–350	6.2	5.49	285	9320–10360
GaN	250–400	3.4	2.13	130	6780–8070

field limits, high carrier mobilities, and strong piezoelectricity [1]–[4]. In addition, their excellent mechanical properties and chemical inertness make them suitable for applications at high temperatures and in harsh environments [5], [6]. Endowed with high elastic modulus and piezoelectricity (see Table I), GaN has recently stimulated growing interests in microelectromechanical systems (MEMS) [7]–[9]. GaN thin-film bulk acoustic resonator (FBAR) and MEMS resonator with integrated high electron mobility transistor (HEMT) channel have been demonstrated, suggesting new opportunities for addressing the filter requirements for the 5G frequency bands [10]–[12]. However, the difficulty in manufacturing native GaN substrates that are desirable to have both high thermal conductivity and low lattice mismatch with GaN epilayers, still presents major limitations for wide and rapid spreading of GaN devices [13]. Tremendous efforts have been put into the growth of GaN epitaxial films on sapphire and silicon carbide (SiC) substrates [14]–[16]. Sapphire substrate has low thermal conductivity [17], whereas SiC raises cost issues though it is well suited for thermal management [18]. Nowadays, the epitaxial growth of III-nitride films and heterostructures on Si (111) substrates is highly attractive owing to the availability of the low-cost and large-size Si substrates, compatibility with standard Si processes, as well as the potential for integration with Si-based devices [19], [20]. Unfortunately, compared with sapphire and SiC substrates, the growth of GaN on Si is limited by the large lattice mismatch and thermal expansion coefficient (TEC) mismatch between GaN and Si, which may result in tensile stress during the process of cooling down from the quite high growth temperature [21].

To address this issue, as depicted in Fig. 1a, a thin, relatively low-temperature, AlN intermediate layer is usually grown as a nucleation layer, eliminating the threading dislocations and generating compressive stress at the growth temperature [22], [23]. However, when the substrate is cooled down to

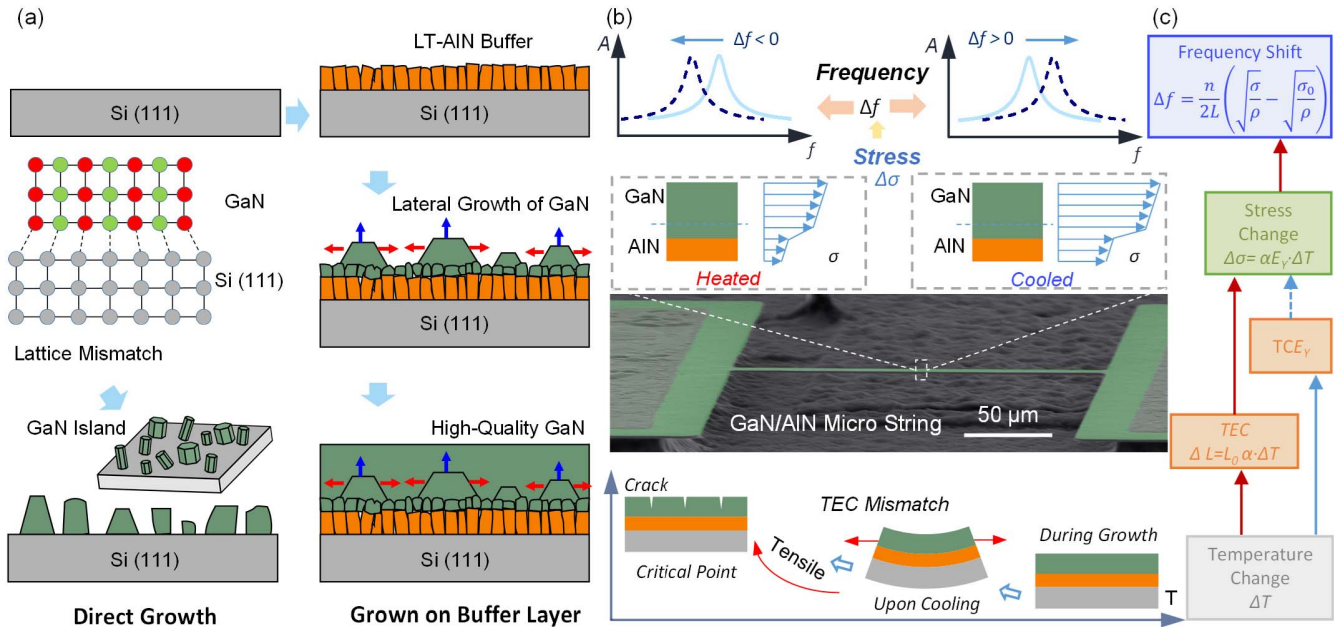


Fig. 1. Scientific background and experimental design. (a) High-quality GaN can be grown on Si (111) substrate by first growing a low temperature (LT) AlN buffer layer as the nucleation layer. (b) Cross-sectional diagrams of the GaN/AlN heterostructure during growth of device layers and upon cooling down back to room temperature. Illustrations show cross-sectional stress distribution and frequency shift of a GaN/AlN heterostructure doubly-clamped micro string resonator with varying temperature. (c) Block diagram showing effects of varying temperature on the resonance frequency.

room temperature after growth, GaN layer shrinks more than Si substrate does, due to its relatively larger thermal expansion coefficient [24] (see Fig. 2a). If the curvature of the substrate induces stress that exceeds the limit of the mechanical strength of the crystalline layer grown on top, the GaN layer will have cracks (see Fig. 1b). Determined by the epitaxial layer sequence grown before the GaN layer, the residual stress can vary significantly within the layer [25]. Adding an intermediate stress compensation layer can introduce compressive stress during the growth, but it is still difficult to completely compensate the excessive tensile stress in GaN resulting from the thermal expansion mismatch [26]. Figure 2c shows the stress evolution within the stack layers during the whole process of temperature ramping up, growth, as well as cooling down. The stress evolution includes four stages. The tensile stress during Stage 1 can be ascribed to the temperature gradient across the Si substrate along the growth direction. When the AlN buffer layer is grown on the Si substrate (Stage 2), the wafer curvature gradually decreases due to the compressive stress generated within the layer. Similarly, the curvature further decreases as the GaN layer grows during Stage 3. Upon cooling down (Stage 4), the compressive stress is compensated by the thermal tensile stress. The residual tensile stress and dislocations in the GaN epilayers and GaN/AlN hetero-layers after cooling down could play a key role in affecting the MEMS resonators and their performance, especially for applications at high temperatures [27]. For a tensioned string without a neutral plane (no plane or line in the string is at zero strain/stress, as strain profile over the cross-section is all positive, *unlike* in beam bending), the maximum tensile stress during vibration occurs periodically when the string has the largest transverse displacement (Fig. 2d & 2e). As temperature varies, the initial tensile stress of the string will be reset

(as a new 'operating point' for a given new temperature). Figure 2d shows the effect of temperature on the stress evolution for a GaN/AlN heterostructure doubly-clamped string resonator under DC and AC mode operations. However, how does the residual tensile stress evolve with temperature and how does this affect the thermal stability of MEMS resonators are still elusive, and remain open questions in the field. Such effects can be assessed by the temperature coefficient of frequency (TC_f) [28]. Essentially, the varying temperature will alter stress (σ) and Young's modulus (E_Y), due to thermal expansion and constitutive crystals' temperature dependence of E_Y , respectively, and change the resonance frequency of MEMS resonator (see Fig. 1c). However, the combined effect of both stress and Young's modulus makes it challenging to *quantitatively* determine the contribution from either of them, especially for MEMS devices with complex structures and heterogeneous materials.

In this work, we build simple doubly-clamped micro string resonators based on GaN/AlN heterostructures on Si (111) substrate, with the resonance frequency dominated by the stress level (not depending on E_Y). We present the first measurement of the TC_f for both out-of-plane and in-plane flexural resonance modes in GaN/AlN doubly-clamped micro string resonators by monitoring the temperature dependence of frequency, over a wide temperature range, from -10 °C up to 325 °C. We fabricate the micro string resonators by a two-step lithography process and measure the resonance response upon temperature change of the device using an ultrasensitive laser interferometry system. The investigation of TC_f may provide helpful insight into analyzing how fluctuations in temperature can affect the characteristics and performance of GaN/AlN resonators with residual (built-in) tensile stress.

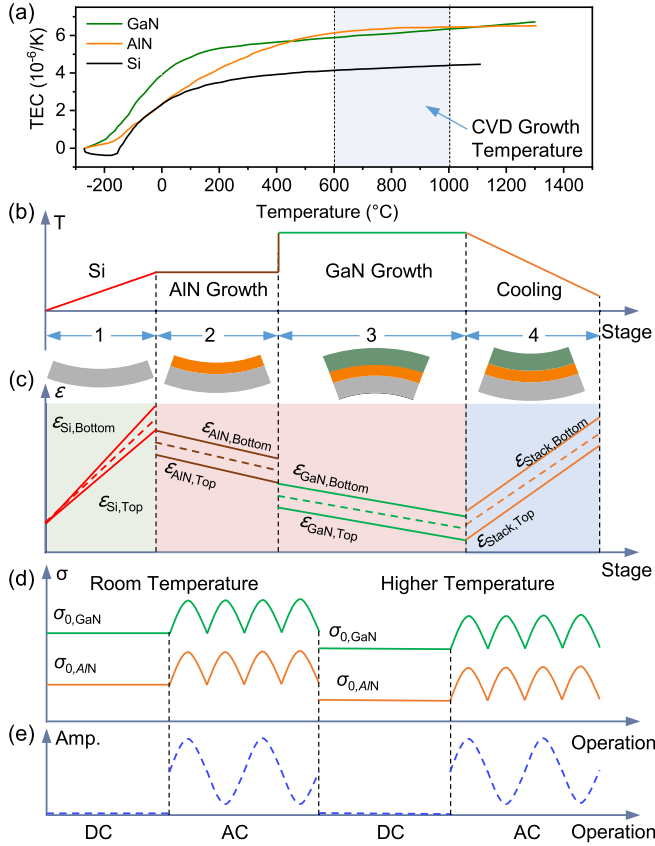


Fig. 2. (a) Thermal expansion coefficient (TEC) of GaN, AlN, and Si. (b) Relative temperature of the whole process including ramping up (Stage 1), growth of AlN (Stage 2) and GaN (Stage 3), and cooling down (Stage 4). (c) Strain evolution in different stages. The dashed lines represent the average strain. Cross-sectional diagrams of the GaN/AIN heterostructure after stage 1, 2, 3, and 4, respectively. (d) Stress evolution and (e) vibration amplitude of a GaN/AIN doubly-clamped string resonator operated under DC (static) and AC (resonance) modes at room temperature and higher temperature, respectively.

II. ANALYTICAL MODELING

The multimode flexural resonance frequencies of a lithographically patterned micro string can be expressed as

$$f_n = \frac{n}{2L} \sqrt{\frac{\sigma}{\rho}} = \frac{n}{2} \sqrt{\frac{\sigma wt}{\rho wt L^2}} = \frac{n}{2} \sqrt{\frac{\sigma wt}{ML}}, \quad (1)$$

where n is the mode number, L is the length of the device, σ is the built-in stress [N/m^2 or Pa] in the string, ρ is the mass density, w is the width, t is the thickness and M is the mass. As suggested by Eq. (1), if the resonance frequencies of the same device have the ratios of 1:2:3..., the resonance frequencies of such modes of the resonator are dominated by the built-in stress (σ) in the device (independent of E_Y) and follow the string model in Eq. (1). Furthermore, the resonance frequency of the same mode (same n) of different devices should be inversely proportional to length L given the built-in stress in the same thin film. By checking the resonance frequency of the same mode of devices with different lengths, we can extract the built-in stress in the devices. To better understand the resonance behavior, we build GaN/AIN doubly-clamped micro string resonators with the lengths of $L = 100 \mu m$, $200 \mu m$ and $300 \mu m$, respectively,

TABLE II

RESONANT FREQUENCIES OF THE FIRST THREE OUT-OF-PLANE MODES

	f_1 (MHz)	f_2 (MHz)	f_3 (MHz)	$f_1: f_2: f_3$
200 μm	0.833	1.676	2.554	$\sim 1: 2: 3$
300 μm	0.547	1.102	1.654	$\sim 1: 2: 3$

and measure their multimode resonances. By tracking the temperature dependence of these resonance modes, we can *quantitatively* determine the TCf, stress level, and thermal expansion coefficient of the resonators. TCf values can be evaluated by using

$$TCf = \frac{1}{f} \frac{df}{dT}, \quad (2)$$

where T is temperature. As temperature varies, the string's dimensions and built-in stress change due to thermal expansion, which shifts the resonance frequencies. The effect of thermal expansion can be described by deformation and stress modification of the string using the equations below:

$$\begin{aligned} w &= w_0 (1 + \alpha T) \\ t &= t_0 (1 + \alpha T) \\ L &= L_0 (1 + \alpha_{Si} T) \\ \sigma &= \sigma_0 - (\alpha - \alpha_{Si}) E_Y T, \end{aligned} \quad (3)$$

where α and E_Y are the thermal expansion coefficient (TEC) and Young's modulus of the GaN/AIN heterostructure, respectively. α_{Si} is the thermal expansion coefficient of Si, with $\alpha_{Si} = 2.6 \text{ ppm}/^{\circ}C$ [29]. Here $E_Y = (E_{Y,GaN} t_{GaN} + E_{Y,AlN} t_{AlN}) / (t_{GaN} + t_{AlN})$. Note that the effect of TCE_Y is not considered due to its negligible effect. By combining Eqs. (1)-(3), we have

$$TCf = \frac{1}{f} \frac{df}{dT} \approx -\frac{1}{2} \alpha_{Si} - \frac{(\alpha - \alpha_{Si}) E_{Y0}}{2\sigma_0}, \quad (4)$$

Here E_{Y0} is the Young's modulus of the GaN/AIN heterostructure at room temperature ($T = 300K$). Based on Eq. (1), we can trace the evolution of stress by tracking the resonance frequencies of the devices as temperature is varied.

III. DEVICE FABRICATION

We use GaN/AIN wafers (purchased from Kyma Technologies, Inc.) that consist of a crystalline GaN layer (500 nm) grown by hydride vapor phase epitaxy (HVPE) on top of an intermediate nucleation layer of AlN (200 nm) on standard Si (111) substrate. As illustrated in Fig. 3, the fabrication of GaN/AIN strings starts from the deposition of chromium (Cr), followed by photolithography to define the Cr hard mask. We perform dry anisotropic etching with the Cr mask, through GaN and AlN layers, to define the doubly-clamped structures, followed by wet etching of Cr. After removal of Cr, we deposit and pattern the titanium (Ti) and aluminum (Al) electrode pads. Finally, we release the GaN/AIN heterostructure devices by isotropic dry etching of Si in xenon difluoride (XeF_2) [30]. Fig. 3 displays an SEM image of as-fabricated devices, with thickness $t = 700 \text{ nm}$, width $w = 5 \mu m$, and length $L = 100, 200$ and $300 \mu m$.

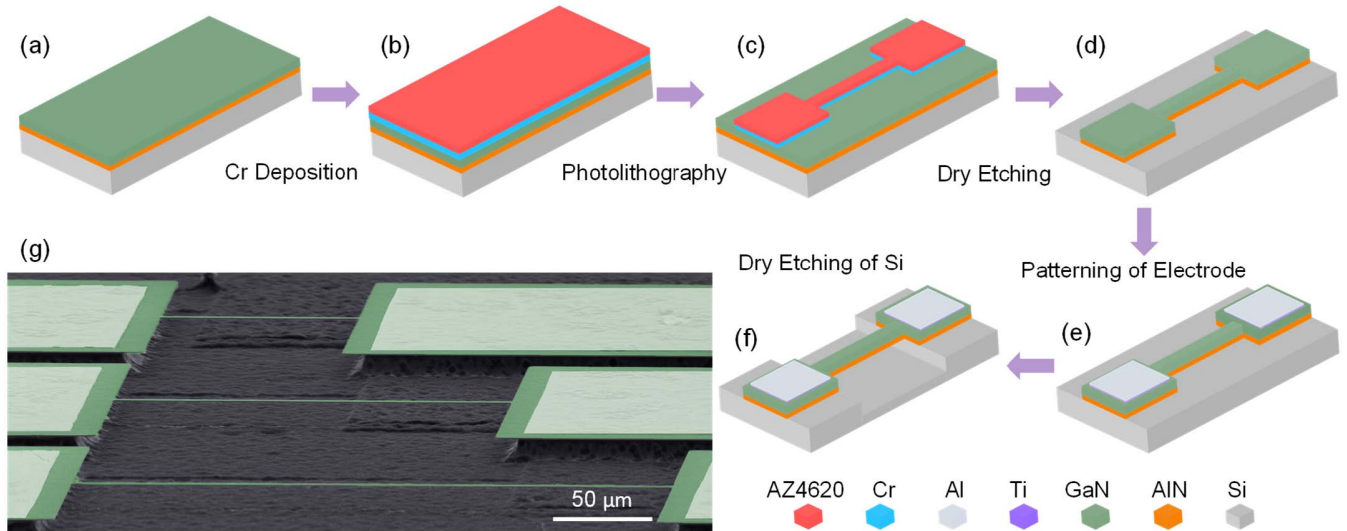


Fig. 3. (a)-(f) Microfabrication of the doubly-clamped GaN/AlN structures via a two-step lithographic process followed by device release in XeF_2 dry etching. (g) An SEM image of suspended GaN/AlN heterostructure micro strings with various lengths.

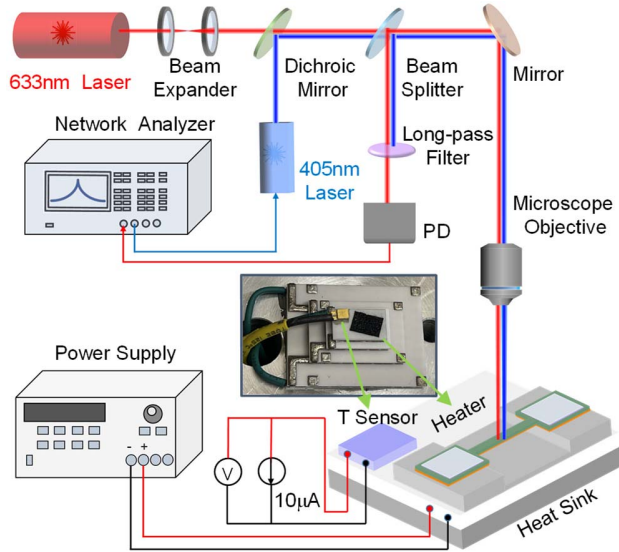


Fig. 4. Illustration of the ultrasensitive laser interferometry measurement system configured with a precisely temperature-controlled device stage.

IV. MEASUREMENT TECHNIQUES

The multimode resonances of the GaN/AlN devices are measured by using a laser interferometry system, as shown in Fig. 4. An intensity-modulated 405 nm blue diode laser is utilized to photo thermally drive the device motion, and a 633 nm He-Ne laser is employed to detect the vibration. Dynamic interference happens between the light reflected by the vibrating string and that by the substrate surface below the suspended structure. Thus, the motion of the device is transduced by the interferometric effect into intensity variation of the reflected 633 nm light. The photodetector converts the optical signal into electrical signal, which is monitored by a network analyzer. We regulate the temperature of the GaN/AlN device by using a Peltier thermoelectric heater/cooler; and the temperature of the chip is measured by a Si diode temperature sensor (Lake Shore DT-670). We measure the resonance responses of the devices at different temperatures,

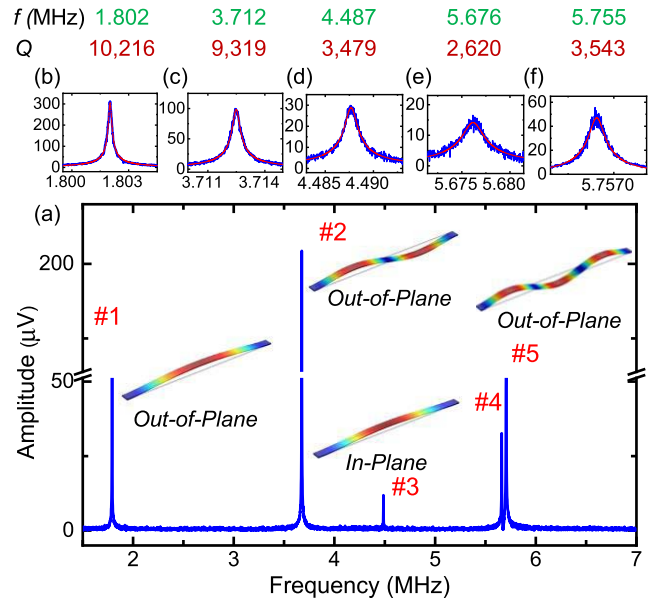


Fig. 5. (a) Measured resonance spectra of a $100\mu\text{m}$ -long GaN/AlN string at room temperature, with panels (b)-(f) showing the zoom-in spectra of 5 modes with fitting curves. Insets show the corresponding simulated mode shapes.

and extract the resonance frequency and quality factor (Q) of each mode by fitting the measured spectrum to the damped simple harmonic resonator model. All the measurements are performed in a moderate vacuum of ~ 80 mTorr [30].

V. RESULTS AND DISCUSSIONS

A. Effects of Resonance Modes on $\text{TC}f$

To study the effects of resonance modes on $\text{TC}f$, we first characterize the multimode resonance of a $100\mu\text{m}$ -long device, including both out-of-plane and in-plane modes. Figure 5 shows the multimode resonances of the $100\mu\text{m}$ -long device measured at room temperature. Five resonance modes are observed in the range of 1.5 to 7 MHz, specifically, $f_1 = 1.802$ MHz, $f_2 = 3.712$ MHz, $f_3 = 4.487$ MHz, $f_4 = 5.676$ MHz, $f_5 = 5.755$ MHz. By matching the resonance

TABLE III
COMPARISON OF TC f OF THE REPORTED FLEXURAL-MODE MEMS/NEMS RESONATORS

References	Material	Resonator Type	Device Dimensions	Mode	Temperature (°C)	TC f (ppm/°C)	Q	Excitation /Detection Scheme
Montague 2012 ^[33]	GaN	Nanowire	3.5 $\mu\text{m} \times 100 \text{ nm}$	Flexural	-261 to 47	40	$\sim 10^5$	Piezoelectric /Homodyne
Yang 2019 ^[34]	AlN	Cantilever	450 $\mu\text{m} \times 20 \mu\text{m} \times 2.05 \mu\text{m}$	Flexural	0 to 50	50.6	$\sim 10^3$	Piezoelectric /Electrical
Boyd 2013 ^[35]	Si	Cantilever	500 $\mu\text{m} \times 50 \mu\text{m} \times 25 \mu\text{m}$	Flexural	-73-27	-23.6 to -26.6	-	Piezoelectric /Optical
Sansa 2016 ^[36]	Si	Cantilever	3.2 $\mu\text{m} \times 300 \text{ nm} \times 160 \text{ nm}$	Flexural	10-40	-38.2	$\sim 10^3$	Electrical /Piezoresistive
Feng 2007 ^[37]	Si	Nanowire	L : 1.69 to 2.25 μm d : 74 to 162 nm	Flexural	-253 to -173	50 to 60	$\sim 10^3$ to 10^5	Magnetomotive Transduction
Koumela 2012 ^[38]	Si	Rectangular Nanowire	3.5 $\mu\text{m} \times 80 \text{ nm} \times 160 \text{ nm}$	Flexural	-269-27	40	$\sim 10^3$	Electrical /Electrical
Boyd 2013 ^[35]	3C-SiC	Cantilever	125 $\mu\text{m} \times 18 \mu\text{m} \times 2.6 \mu\text{m}$	Flexural	-73-27	-16 to -21	-	Piezoelectric /Optical
Pozzi 2007 ^[39]	3C-SiC	Cantilever	L : 50-500 μm w : 20 or 30 μm t : 2.7 μm	Flexural	22-600	-25	-	Electrostatic /Optical
Chung 2009 ^[40]	3C-SiC	Cantilever	L : 60, 80, 100 μm w : 10 μm t : 1.2 μm	Flexural	25-200	-9.79 -7.72 -8.0	-	Piezoelectric /Optical
Chung 2009 ^[40]	3C-SiC	Doubly Clamped Beam	L : 60, 80, 100 μm w : 10 μm t : 0.4 μm	Flexural	25-200	-15.74 -12.55 -8.35	-	Piezoelectric /Optical
Chuang 2004 ^[41]	SiN	T-Shape Cantilever	L_a : 155 μm w_a : 20 μm L_b : 50 μm w_b : 60 μm	Flexural	-243-25	-57.35	2050	Electron Beam /Piezoelectric
This Work	GaN/AlN	Doubly Clamped Structure	L : 100, 200, 300 μm w : 5 μm t : 700 nm	Flexural	-10-325	-83 to -512	$\sim 10^3$ to 10^4	Optical/Optical

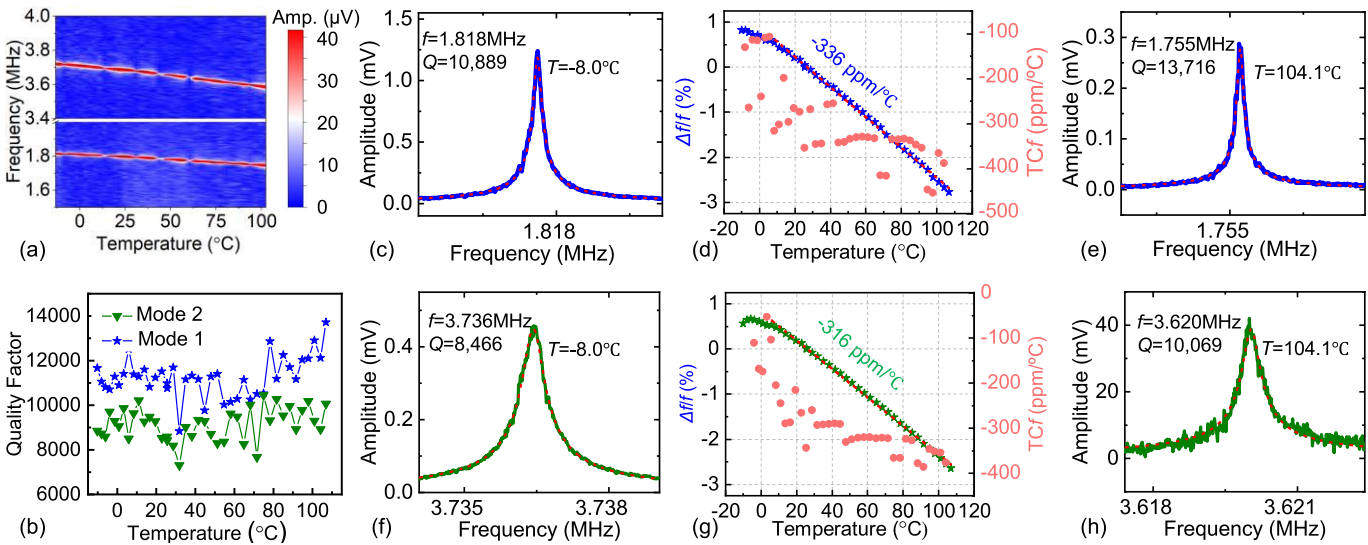


Fig. 6. The first two out-of-plane resonance modes and TC f measured from a device with length $L = 100 \mu\text{m}$. (a) Color plot of the resonance spectra for the first two modes measured with varying temperature. (b) Measured Q versus temperature. Measured (c) first mode and (f) second mode resonances at -8.0°C . (d) and (g) Fractional frequency shift with varying temperature. Measured (e) first mode and (h) second mode resonance at 104.1°C .

frequencies to finite element method (FEM) simulation results, the first two modes are out-of-plane flexural modes while the third one is an in-plane flexural mode. Between the measured fourth and fifth modes, one of them is the third out-of-plane flexural mode.

We first characterize the TC f of the out-of-plane modes. Figure 6 shows the resonance spectra of the first two modes measured in temperature range of -10 to 105°C . We find that

the resonance frequencies increase gradually with decreasing temperatures. By plotting the frequency shift at different temperatures with respect to its resonance frequency at 25.6°C for each mode (Fig. 6d & 6g), we observe linear relation between $\Delta f/f$ and T among most of the measured temperatures. In this range, we extract an average TC f_1 of $-336 \text{ ppm}/^\circ\text{C}$ for the fundamental mode and TC f_2 of $-316 \text{ ppm}/^\circ\text{C}$ for the second mode. No clear trend of Q change is

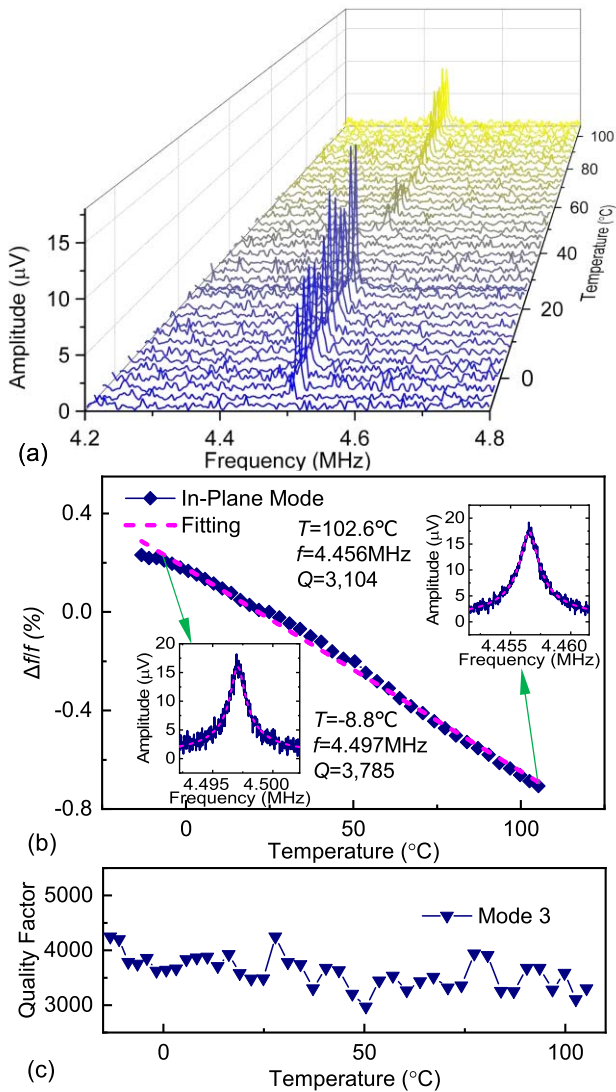


Fig. 7. Measured in-plane flexural mode resonance and TCf. (a) Resonance spectra at different temperatures from -10 to 105°C . (b) Fractional frequency shift versus temperature. *Insets* show resonance spectra at selected temperatures. (c) Measured Q versus temperature.

observed (Fig. 6b). According to the frequency ratio of the first two modes ($f_2/f_1 \approx 2$), the out-of-plane modes can be precisely described by using the string model (with $\sigma \approx 700$ MPa). Based on Eq. (4), we obtain $\alpha \approx 3.9$ ppm/ $^{\circ}\text{C}$, which is comparable to the thermal expansion coefficient values of GaN (~ 2.0 – 3.8 ppm/ $^{\circ}\text{C}$) and AlN (~ 4.2 – 5.3 ppm/ $^{\circ}\text{C}$) from literature [31], [32].

To further investigate frequency response of the GaN/AlN doubly-clamped structure, we also measure the temperature dependence of the first in-plane (lateral) flexural mode (3^{rd} mode overall, f_3). Figure 7a shows resonance spectra of the 3^{rd} mode as the device temperature is regulated over $T = -10$ to 105°C . We observe much smaller frequency shift as temperature varies (than in the earlier two modes). It is further confirmed by Fig. 7b, where f responds linearly to sweeping T in the measured T range with an averaged $\text{TC}f_3 = -83$ ppm/ $^{\circ}\text{C}$, less than 1/3 of earlier measured values for out-of-plane modes ($\text{TC}f_1$ and $\text{TC}f_2$). Based on the cross-sectional shape (rectangular) and orientation of the

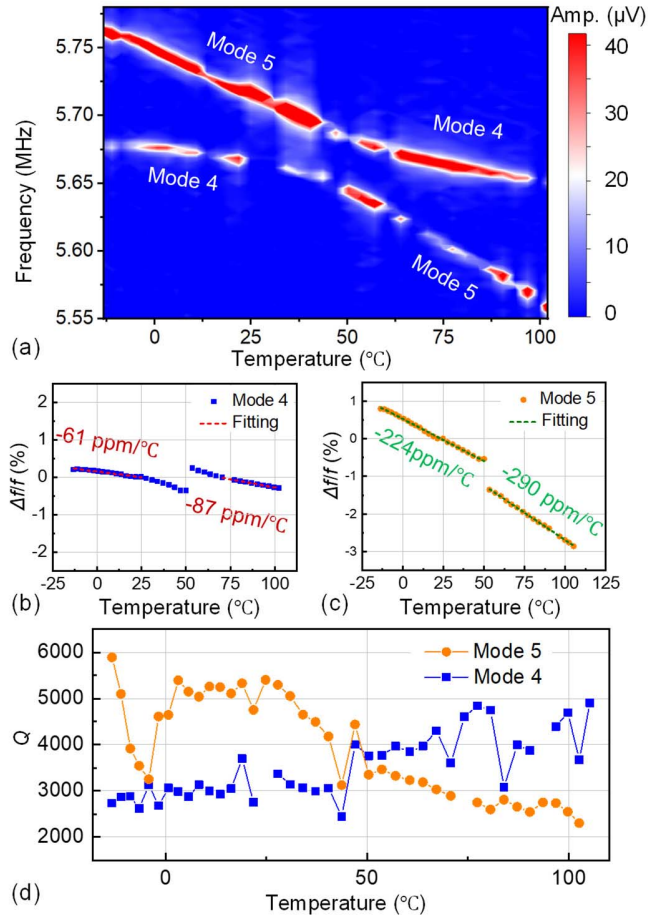


Fig. 8. Measured resonance characteristics of the 4^{th} and 5^{th} flexural modes and TCf. (a) Resonance spectra at different temperatures from -10 to 105°C . Fractional frequency shift versus temperature for (b) the 4^{th} mode and (c) the 5^{th} mode. (d) Measured Q versus temperature, for both the 4^{th} and 5^{th} modes.

doubly-clamped structure, the flexural rigidity in the in-plane direction ($E_Y I_z = E_Y t w^3/12$) is more than fifty time larger than that in the out-of-plane direction ($E_Y I_z = E_Y w t^3/12$). Thus, the in-plane mode resonance frequency, f_3 , depends more on E_Y of the material than on the built-in stress σ , compared to the two out-of-plane flexural modes (f_1 and f_2). The shift of resonance frequency caused by the change of built-in stress (induced by thermal expansion) can be partly compromised by the frequency modulation induced by Young's modulus change (governed by TCE_Y), leading to a smaller TCf for the in-plane mode. The Q of the in-plane mode is also generally stable, with minor declination, over the varying temperature range (Fig. 7c) [30].

Figure 8a shows the frequencies of both the 4^{th} and 5^{th} modes as functions of temperature, in which we observe a clear effect of anti-crossing between the 4^{th} and 5^{th} modes. The anti-crossing point appears at $\sim 50^{\circ}\text{C}$. At the anti-crossing, the higher frequency of the 5^{th} mode drops down, while the lower frequency of the 4^{th} mode goes higher. Above the anti-crossing point, *i.e.*, in the higher temperature region, the TCf values of both modes are slightly larger than those in the lower temperature region as shown in Fig. 8b & 8c. The average TCf for the 4^{th} mode is about -74 ppm/ $^{\circ}\text{C}$ and the average TCf for the

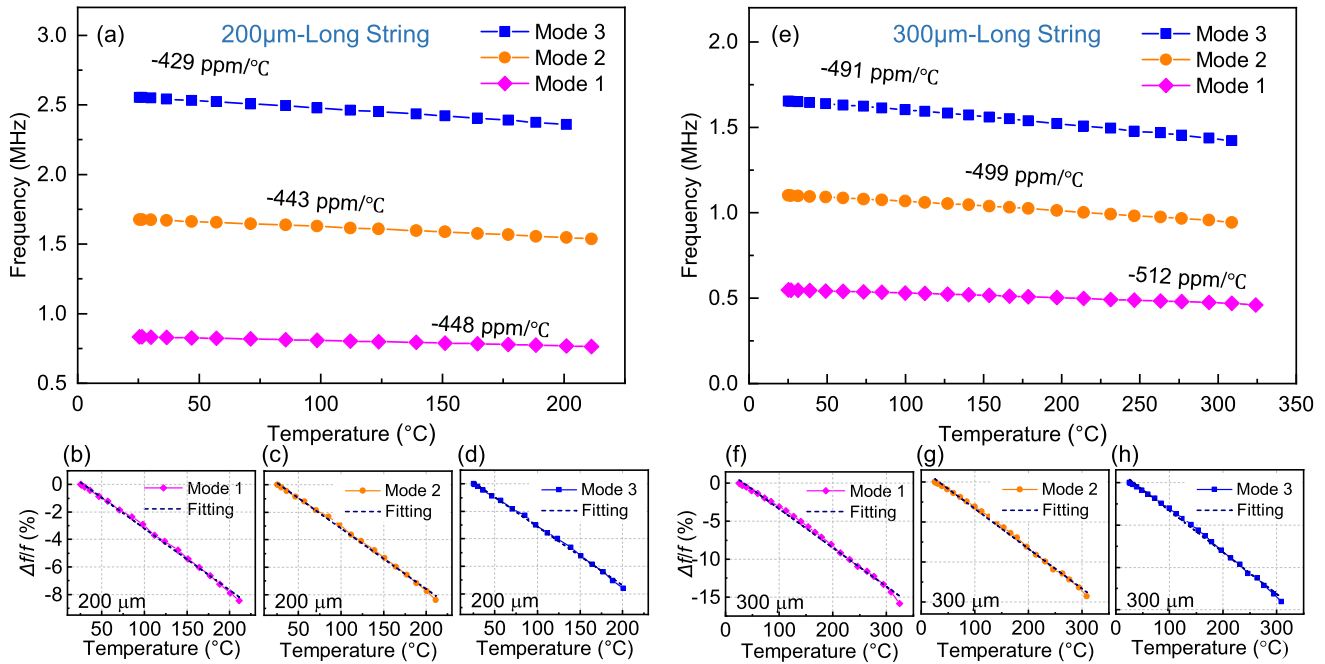


Fig. 9. Measured out-of-plane flexural mode resonances and TC f values. (a) Resonance spectra of 200 μm -long device at different temperatures from 25 to 225 $^{\circ}\text{C}$. (b) to (d) Fractional frequency shift versus temperature. (e) Resonance spectra of 300 μm -long device at different temperatures from 25 to 325 $^{\circ}\text{C}$. (f) to (h) Fractional frequency shift versus temperature.

5th mode is about -250 ppm/ $^{\circ}\text{C}$. According to the TC f values, we infer the anti-crossing occurs between an in-plane mode (4th mode) and an out-of-plane mode (5th mode). In contrast to the Q curves of the first three modes, the measured Q of the 4th mode increases, while the Q of the 5th mode declines overall, in the temperature range of -10 to 105 $^{\circ}\text{C}$ (see Fig. 8d).

B. Effects of Device Length on TC f

We further study the temperature dependence of frequency of GaN/AlN heterostructure devices with lengths of 200 μm and 300 μm in higher temperature range (with the highest temperature up to 325 $^{\circ}\text{C}$). Table II summarizes the resonance frequencies and frequency ratios of the first three out-of-plane modes. According to the frequency ratios, the out-of-plane modes can be precisely described by the string model in Eq. (1).

As shown in Fig. 9, the frequency decreases almost linearly with the temperature increase for all three out-of-plane modes. We have extracted the TC f values as well. For both 200 μm -long and 300 μm -long devices, only subtle differences of TC f values are observed among different out-of-plane modes. Although the TC f value should be independent of the length of device according to the simplified theoretical analysis (Eq. (4)), we observe the longer devices indeed have larger TC f values. For 200 μm -long one, the TC f value is centered at about -440 ppm/ $^{\circ}\text{C}$, and the 300 μm -long one exhibits a larger TC f of about -500 ppm/ $^{\circ}\text{C}$. This suggests the built-in stress in the longer device may be smaller than that in the shorter device. Detailed comparisons of TC f between this work and the reported flexural-mode MEMS/NEMS resonators are summarized in Table III. We can find that compared with those devices, the GaN/AlN heterostructure doubly-clamped

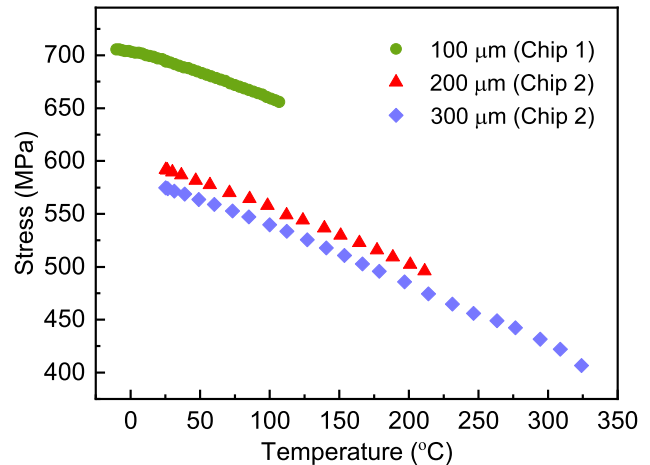


Fig. 10. The evolution of tensile stress with varying temperature for the devices with lengths $L = 100, 200$ and 300 μm .

micro-string resonators in this work offer the highest TC f values up to -512 ppm/ $^{\circ}\text{C}$. These very linear dependence curves and TC f values can be exploited for thermal sensing (*e.g.*, detection of radiation-induced thermal absorption, such as ultraviolet (UV) light or gamma ray).

According to the measured resonance frequency and Eq. (1), we have extracted the evolution of tensile stress at varying temperature as shown in Fig. 10. The 100 μm -long string from Chip 1 exhibits higher level of initial stress of ~ 700 MPa than longer devices on Chip 2 with the initial stress lying between 500 to 600 MPa. As the temperature increases, the tensile stresses are gradually released due to the different thermal expansion of GaN and Si. For the 300 μm -long string, stress has relaxed from 575 MPa to 400 MPa as temperature is increased from 25 $^{\circ}\text{C}$ to 325 $^{\circ}\text{C}$. Interestingly, amongst these

devices, the 300- μm -long string exhibits the lowest initial stress ($\sim 550\text{MPa}$) but the largest $\text{TC}f$ value ($-512\text{ ppm}/^\circ\text{C}$). Comparison of $\text{TC}f$ and tensile stress among the three devices, we can conclude that higher tensile stress levels contribute to smaller $\text{TC}f$ values.

VI. CONCLUSION

In summary, we have designed GaN/AlN heterostructure micro string resonators with lengths $L = 100, 200$ and $300\ \mu\text{m}$ to probe the stress and thermal effects on resonance behavior. The resonances of out-of-plane modes show clear string behavior. By tracking the temperature dependence of multimode resonances, we have found the frequencies downshift almost linearly with increasing temperature up to $325\ ^\circ\text{C}$. For a given device, the out-of-plane modes show similar $\text{TC}f$ values, which are three times larger than that of the in-plane mode. The longer devices tend to have larger $\text{TC}f$ values. We observe the largest $\text{TC}f$ value of about $-500\text{ ppm}/^\circ\text{C}$ in a 300- μm -long device. The linear temperature dependence and $\text{TC}f$ values of GaN/AlN heterostructure resonators can be directly employed for thermal sensing. Comparison among different devices indicates that the residual stress in GaN/AlN heterostructures plays a key role in affecting the $\text{TC}f$ values. Higher tensile stress levels contribute to smaller measured $\text{TC}f$ values. Strain engineering may thus be employed to regulate the $\text{TC}f$ of MEMS devices.

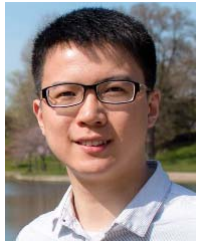
REFERENCES

- [1] O. Ambacher, "Growth and applications of group III-nitrides," *J. Phys. D, Appl. Phys.*, vol. 31, no. 20, pp. 2653–2710, Oct. 1998.
- [2] S. P. DenBaars *et al.*, "Development of gallium-nitride-based light-emitting diodes (LEDs) and laser diodes for energy-efficient lighting and displays," *Acta Mater.*, vol. 61, no. 3, pp. 945–951, Feb. 2013.
- [3] M. Faucher *et al.*, "Amplified piezoelectric transduction of nanoscale motion in gallium nitride electromechanical resonators," *Appl. Phys. Lett.*, vol. 94, no. 23, Jun. 2009, Art. no. 233506.
- [4] T. Zimmermann *et al.*, "Piezoelectric GaN sensor structures," *IEEE Electron Device Lett.*, vol. 27, no. 5, pp. 309–312, May 2006.
- [5] A. Hassan, Y. Savaria, and M. Sawan, "GaN integration technology, an ideal candidate for high-temperature applications: A review," *IEEE Access*, vol. 6, pp. 78790–78802, 2018.
- [6] S. Faramehr, N. Jankovic, and P. Igetic, "GaN current transducers for harsh environments," in *Proc. 20th Int. Conf. Solid-State Sensors, Actuators, Microsyst. Eurosens. XXXIII (TRANSDUCERS EUROSENSORS XXXIII)*, Jun. 2019, pp. 1985–1988.
- [7] M. Rais-Zadeh *et al.*, "Gallium nitride as an electromechanical material," *J. Microelectromech. Syst.*, vol. 23, no. 6, pp. 1252–1271, Dec. 2014.
- [8] M. Rais-Zadeh, H. Zhu, and A. Ansari, "Applications of gallium nitride in MEMS and acoustic microsystems," in *Proc. IEEE 17th Topical Meeting Silicon Monolithic Integr. Circuits RF Syst. (SiRF)*, Jan. 2017, pp. 9–11.
- [9] M. Faucher, Y. Cordier, M. Werquin, L. Buchaillot, C. Gaquiere, and D. Theron, "Electromechanical transconductance properties of a GaN MEMS resonator with fully integrated HEMT transducers," *J. Microelectromech. Syst.*, vol. 21, no. 2, pp. 370–378, Apr. 2012.
- [10] A. Müller *et al.*, "6.3-GHz film bulk acoustic resonator structures based on a gallium nitride/silicon thin membrane," *IEEE Electron Device Lett.*, vol. 30, pp. 799–809, Aug. 2009.
- [11] A. Ansari, V. J. Gokhale, V. A. Thakar, J. Roberts, and M. Rais-Zadeh, "Gallium nitride-on-silicon micromechanical overtone resonators and filters," in *IEDM Tech. Dig.*, Dec. 2011, pp. 485–488.
- [12] A. Ansari, V. J. Gokhale, J. Roberts, and M. Rais-Zadeh, "Monolithic integration of GaN-based micromechanical resonators and HEMTs for timing applications," in *IEDM Tech. Dig.*, Dec. 2012, pp. 363–366.
- [13] T. Paskova, D. A. Hanser, and K. R. Evans, "GaN substrates for III-nitride devices," *Proc. IEEE*, vol. 98, no. 7, pp. 1324–1338, Jul. 2010.
- [14] I. Akasaki, "Nobel lecture: Fascinated journeys into blue light," *Rev. Modern Phys.*, vol. 87, no. 4, pp. 1119–1131, Oct. 2015.
- [15] J. N. Kuznia, M. A. Khan, D. T. Olson, R. Kaplan, and J. Freitas, "Influence of buffer layers on the deposition of high quality single crystal GaN over sapphire substrates," *J. Appl. Phys.*, vol. 73, no. 9, pp. 4700–4702, May 1993.
- [16] R. Gaska, Q. Chen, J. Yang, A. Osinsky, M. Asif Khan, and M. S. Shur, "High-temperature performance of AlGaIn/GaN HFETs on SiC substrates," *IEEE Electron Device Lett.*, vol. 18, no. 10, pp. 492–494, Oct. 1997.
- [17] S. G. Nassif-Khalil and C. A. T. Salama, "Super-junction LDMOST on a silicon-on-sapphire substrate," *IEEE Trans. Electron Devices*, vol. 50, no. 5, pp. 1385–1391, May 2003.
- [18] N. Kaminski and O. Hilt, "SiC and GaN devices—Wide bandgap is not all the same," *IET Circuits, Devices Syst.*, vol. 8, no. 3, pp. 227–236, May 2014.
- [19] J. D. Brown, R. Borges, E. Piner, A. Vescan, S. Singhal, and R. Therrien, "AlGaIn/GaN HFETs fabricated on 100-mm GaN on silicon (111) substrates," *Solid-State Electron.*, vol. 46, no. 10, pp. 1535–1539, Oct. 2002.
- [20] T. Boles, "GaN-on-silicon present challenges and future opportunities," in *Proc. 12th Eur. Microw. Integr. Circuits Conf. (EuMIC)*, Oct. 2017, pp. 21–24.
- [21] T. Boles, "GaN-on-silicon-present capabilities and future directions," *AIP Conf. Proc.*, vol. 1934, no. 1, Feb. 2018, Art. no. 020001.
- [22] Y. Fu, D. A. Gulino, and R. Higgins, "Residual stress in GaN epilayers grown on silicon substrates," *J. Vac. Sci. Technol. A, Vac., Surf., Films*, vol. 18, no. 3, pp. 965–967, May 2000.
- [23] A. Watanabe, T. Takeuchi, K. Hirotsawa, H. Amano, K. Hiramatsu, and I. Akasaki, "The growth of single crystalline GaN on a Si substrate using AlN as an intermediate layer," *J. Cryst. Growth*, vol. 128, nos. 1–4, pp. 391–396, Mar. 1993.
- [24] S. Q. Zhou, A. Vantomme, B. S. Zhang, H. Yang, and M. F. Wu, "Comparison of the properties of GaN grown on complex Si-based structures," *Appl. Phys. Lett.*, vol. 86, no. 8, Feb. 2005, Art. no. 081912.
- [25] A. Able, W. Wegscheider, K. Engl, and J. Zweck, "Growth of crack-free GaN on Si(111) with graded AlGaIn buffer layers," *J. Cryst. Growth*, vol. 276, nos. 3–4, pp. 415–418, Apr. 2005.
- [26] N. Baron *et al.*, "The critical role of growth temperature on the structural and electrical properties of AlGaIn/GaN high electron mobility transistor heterostructures grown on Si(111)," *J. Appl. Phys.*, vol. 105, no. 3, Feb. 2009, Art. no. 033701.
- [27] C. Morelle *et al.*, "Gallium nitride MEMS resonators: How residual stress impacts design and performances," *Microsyst. Technol.*, vol. 24, no. 1, pp. 371–377, Jan. 2018.
- [28] A. K. Samarao and F. Ayazi, "Temperature compensation of silicon micromechanical resonators via degenerate doping," in *IEDM Tech. Dig.*, Dec. 2009, pp. 789–792.
- [29] Y. Okada and Y. Tokumaru, "Precise determination of lattice parameter and thermal expansion coefficient of silicon between 300 and 1500 K," *J. Appl. Phys.*, vol. 56, no. 2, pp. 314–320, Jul. 1984.
- [30] W. Sui, X.-Q. Zheng, J.-T. Lin, B. W. Alphenaar, and P. X.-L. Feng, "Temperature dependence of multimode gallium nitride/aluminum nitride (GaN/AlN) heterostructure string resonator," in *Proc. IEEE 34th Int. Conf. Micro Electro Mech. Syst. (MEMS)*, Jan. 2021, pp. 478–481.
- [31] M. Leszczynski *et al.*, "Thermal expansion of gallium nitride," *J. Appl. Phys.*, vol. 76, no. 8, pp. 4909–4911, Oct. 1994.
- [32] W. M. Yim and R. J. Paff, "Thermal expansion of AlN, sapphire, and silicon," *J. Appl. Phys.*, vol. 45, no. 3, pp. 1456–1457, Mar. 1974.
- [33] J. R. Montague, K. A. Bertness, N. A. Sanford, V. M. Bright, and C. T. Rogers, "Temperature-dependent mechanical-resonance frequencies and damping in ensembles of gallium nitride nanowires," *Appl. Phys. Lett.*, vol. 101, no. 17, Oct. 2012, Art. no. 173101.
- [34] J. Yang *et al.*, "A T-shape aluminum nitride thin-film piezoelectric MEMS resonant accelerometer," *J. Microelectromech. Syst.*, vol. 28, no. 5, pp. 776–781, Oct. 2019.
- [35] E. J. Boyd, L. Li, R. Blue, and D. Uttamchandani, "Measurement of the temperature coefficient of Young's modulus of single crystal silicon and 3C silicon carbide below 273 K using micro-cantilevers," *Sens. Actuators A, Phys.*, vol. 198, pp. 75–80, Aug. 2013.
- [36] M. Sansa *et al.*, "Frequency fluctuations in silicon nanoresonators," *Nature Nanotechnol.*, vol. 11, no. 6, pp. 552–558, Jun. 2016.
- [37] X. L. Feng, R. R. He, P. D. Yang, and M. L. Roukes, "Quality factors and energy losses of single-crystal silicon nanowire electromechanical resonators," in *Proc. TRANSDUCERS Int. Solid-State Sensors, Actuators, Microsyst. Conf.*, Jun. 2007, pp. 1325–1326.

- [38] A. Koumela, D. Mercier, C. Marcoux, L. Duraffourg, and S. T. Purcell, "Performances of suspended silicon nanowire resonators for time reference applications," in *Proc. IEEE Int. Freq. Control Symp.*, May 2012, pp. 1–4.
- [39] M. Pozzi *et al.*, "Mechanical properties of a 3C-SiC film between room temperature and 600 °C," *J. Phys. D, Appl. Phys.*, vol. 40, no. 11, pp. 3335–3342, May 2007.
- [40] G. S. Chung and T. W. Lee, "Temperature characteristics of polycrystalline 3C-SiC micro resonators," *J. Korean Inst. Electr.*, vol. 22, no. 4, pp. 314–317, Apr. 2009.
- [41] W.-H. Chuang, T. Luger, R. K. Fetting, and R. Ghodssi, "Mechanical property characterization of LPCVD silicon nitride thin films at cryogenic temperatures," *J. Microelectromech. Syst.*, vol. 13, no. 5, pp. 870–879, Oct. 2004.



Wen Sui (Graduate Student Member, IEEE) received the B.S. and M.S. degrees in mechanical engineering from Northeastern University, Shenyang, China, in 2016 and 2019, respectively. He is currently pursuing the Ph.D. degree with the Department of Electrical and Computer Engineering (ECE), University of Florida, Gainesville, USA. His research interests include nano/microelectromechanical systems (NEMS/MEMS), gallium nitride (GaN) MEMS, and 2D material NEMS devices. He was a recipient of the Margaret A. Ross Fellowship from ECE, University of Florida.



Xu-Qian Zheng (Member, IEEE) received the B.S. degree in mechanical engineering and automation from the Nanjing University of Aeronautics and Astronautics, Nanjing, China, in 2013, and the M.Sc. and Ph.D. degrees in electrical engineering from Case Western Reserve University (CWRU), Cleveland, OH, USA, in 2015 and 2019, respectively. He is currently a Post-Doctoral Research Associate with the Department of Electrical and Computer Engineering, University of Florida, Gainesville, FL, USA. He has published 15 peer-reviewed journal

articles and contributed 13 conference publications. His major research area is ultra-wide-bandgap materials for MEMS/NEMS applications. He also works on the development of piezoelectric MEMS/NEMS, fundamental study of 2D material NEMS devices, and piezoelectric energy harvesting from ambient vibrations. He received the ThinkEnergy Fellowship from the Great Lakes Energy Institute, CWRU, in 2015. He was also a single recipient of the Ruth Barber Moon Award from the Case School of Engineering in 2017, in recognition of his academic promise and leadership. He was a finalist of the Best Student Paper Competition at the 2016 IEEE International Frequency Control Symposium (IFCS 2016) and the Outstanding Paper Award Competition at the 30th IEEE International Conference on Micro Electro Mechanical Systems (MEMS 2017).



Ji-Tzuoh Lin was born in Taipei, Taiwan. He received the M.S. degree in physics and the Ph.D. degree in electrical engineering from the University of Louisville, Louisville, KY, USA, in 2000 and 2006, respectively. His doctoral study was to develop MEMS spinal fusion sensors and their telemetry system.

After graduation, he extended his research interests to the MEMS devices that enable small scale vibrational energy harvesting and micro-explosion. In this period, he was specifically interested in low

power MEMS solutions for sensors and actuators. During the past few years, the focus was turned to radiation detection with MEMS resonators for space application. He held research positions at the University of Louisville for the past 14 years. He is working on research involving optical time of flight (ToF)

sensors and polymer strain gauges, both areas will be used for human interfaces for location and environmental detection. He is currently a Research Engineer with the Louisville Automation and Robotic Research Institute (LARRI), University of Louisville. He has started a company called Ambiharv. He has published two book chapters, 20 peer-reviewed journal publications, and 37 conference presentations and proceedings and one issued patent. He was a recipient of the SBIR Award. He was placed first in the Student Competition in medical and engineering category at Research!Louisville 2004. His article "Magnetic coupling of piezoelectric cantilever for enhanced energy harvesting efficiency" was selected by *Smart Materials and Structures* to the collection of the journal's highlight of the year 2010.



Bruce W. Alphenaar (Member, IEEE) received the B.S. degree in physics from the Trinity College, CT, in 1984, and the Ph.D. degree in applied physics from Yale University in 1991. Starting from 1991, he worked for two years at Philips Research, Eindhoven, The Netherlands, and for eight years at the Hitachi Cambridge Laboratory in collaboration with Hitachi, Japan, and the Cavendish Physics Laboratory, Cambridge University, U.K. Then, he joined the faculty of the Electrical and Computer Engineering Department, University of Louisville, where he became a Professor in 2007. He has extensive research experience in micro/nano technology and has published over 150 research articles. He holds eight U.S. and European patents.



Philip X.-L. Feng (Senior Member, IEEE) received the Ph.D. degree in electrical engineering (EE) from the California Institute of Technology (Caltech), Pasadena, CA, USA, in 2007. He is currently a Professor with the Department of Electrical and Computer Engineering, University of Florida, Gainesville, FL, USA. His research is primarily focused on emerging solid-state devices and systems, particularly nano/microelectromechanical systems (NEMS/MEMS), atomic layer semiconductors and 2D devices, silicon carbide (SiC) and other

advanced semiconductors, quantum devices based on SiC and 2D materials, and their integration with state-of-the-art ICs and optical/photon technologies. He is an alumnus of the National Academy of Engineering (NAE) U.S. Frontier of Engineering (USFOE) Program, and a recipient of the NAE Grainger Foundation Frontiers of Engineering (FOE) Award. His awards also include the Presidential Early Career Award for Scientists and Engineers (PECASE 2019) and the National Science Foundation CAREER Award in 2015. He and his students have won four best paper/presentation awards at IEEE and other international conferences. He has mentored over ten Ph.D. students to successful dissertation defense and also supervised eight M.S. students with thesis research. He has served on the Technical Program Committees (TPCs) for the IEEE International Electron Devices Meeting (IEDM), the IEEE International Conference on Micro Electro Mechanical Systems (MEMS), the International Conference on Solid-State Sensors, Actuators and Microsystems (Transducers), the IEEE International Frequency Control Symposium (IFCS) and European Frequency and Time Forum (EFTF), the IEEE SENSORS, the IEEE NANO, and other international conferences and workshops. He served as the Track Chair for the IEEE SENSORS from 2016 to 2017 and as the TPC Group Chair of the IEEE IFCS 2018, IFCS-EFTF 2019, and IFCS-ISAF 2020. He has also served as the Technical Program Chair of the MEMS/NEMS Technical Group at the 61st to 63rd American Vacuum Society (AVS) International Symposium and Exhibition. He has been a Co-Organizer and the Technical Chair of the SiC Materials and Devices Workshop since 2017. He has served as the Chair of the 34th IEEE International Conference on Micro Electro Mechanical Systems (IEEE MEMS 2021).